Southern Ocean wind stress in CMIP5 models: Role of wind fluctuations

Xia Lin[1,2], Xiaoming Zhai[3], Zhaomin Wang[1,2] and David R. Munday[4]

[1] College of Oceanography, Hohai University, Nanjing, China

[2] International Polar Environment Research Laboratory, Hohai University, Nanjing, China

[3] Centre for Ocean and Atmospheric Sciences, School of Environmental Sciences, University of East Anglia, Norwich, United Kingdom

[4] British Antarctic Survey, Cambridge, United Kingdom

Correspondence to: Xiaoming Zhai (Xiaoming.Zhai@uea.ac.uk) and Zhaomin Wang (Zhaomin.Wang@hhu.edu.cn).

Abstract

The Southern Ocean (SO) surface wind stress is a major atmospheric forcing for driving the Antarctic Circumpolar Current and the global overturning circulation. Here the effects of wind fluctuations at different time scales on SO wind stress in eighteen models from phase 5 of the Coupled Model Intercomparison Project (CMIP5) are investigated. It is found that including wind fluctuations, especially on timescales associated with synoptic storms, in the stress calculation strongly enhances the mean strength, modulates the seasonal cycle, and significantly amplifies the trends of SO wind stress. In eleven out of the eighteen CMIP5 models, the SO wind stress has strengthened significantly over the period of 1960-2005. Among them, the strengthening trend of SO wind stress in one CMIP5 model is due to the increase in the intensity of wind fluctuations, while in all the other ten models the strengthening trend is due to the increasing strength of the mean westerly wind. These discrepancies in SO wind stress trend in CMIP5 models may explain some of the diverging behaviors in the model-simulated SO circulation. Our results suggest that to reduce the uncertainty in SO responses to wind stress changes in the coupled models, both the mean wind and wind fluctuations need to be better simulated.

1. Introduction

The Southern Hemisphere (SH) surface westerly wind stress plays an instrumental role in driving the Southern Ocean (SO) circulation and the global meridional overturning circulation (Marshall and Speer 2012; Meredith et al. 2012; Gent 2016), as well as SO temperature changes and carbon uptake (Le Quéré et al. 2007; Gille, 2008; Wang et al. 2015; Jones et al. 2016; Wang et al. 2017). Since surface wind stress depends nonlinearly on surface wind velocity (e.g. Large et al. 1994), high-frequency wind fluctuations contribute to both the mean strength and low-frequency variability of surface wind stress (Zhai and Wunsch 2013). For example, when wind fluctuations with time scales less than one month are included in the stress calculation, the time-mean wind stress is significantly enhanced, which then leads to an increase in wind power input to the ocean general circulation of over 70% (Zhai et al. 2012; Wu et al. 2016).

Recently, Lin et al. (2018) investigated the contributions of atmospheric wind fluctuations to the mean, variability and trend of SO wind stress over the last four decades using reanalysis products. They found that including wind variability at synoptic frequencies (2-8 days) and higher in the stress calculation increases the strength of the mean SO wind stress by as much as almost 40%. However, large discrepancies exist among reanalysis products regarding the role of wind fluctuations in determining the strengthening trend of SO wind stress; the strengthening trend in ERA-Interim is due entirely to the increasing strength of the mean westerly wind, while between one-third and one-half of the strengthening trend in NCEP is attributable to the increase in the intensity of wind fluctuations (Lin et al. 2018). These large discrepancies are worrying and may explain some of the diverging behaviors of the model-simulated SO circulation and water mass distribution when forced with different reanalysis products (e.g. Zika et al. 2013a, 2013b; Langlais et al. 2015). As highlighted recently by Munday and Zhai (2017), the sensitivity of SO circulation to wind stress changes

depends strongly on how these stress changes are brought about, i.e., whether via changes of the mean wind or changes of wind variability. In their model experiments, when the increase in SO wind stress is made by increasing the intensity of wind variability, vertical mixing and water mass transformation processes are enhanced in the mixed layer, which results in a much greater sensitivity of the SO meridional overturning circulation to the increased wind stress. Therefore, to understand how the climate system may respond to the observed and predicted increase in SO wind stress, it is important to first understand how this increase in wind stress is brought about.

Models from phase 5 of the Coupled Model Intercomparison Project (CMIP5) are widely used to simulate historical and predict future changes of the strength and position of the SO surface westerly winds (Ceppi et al. 2012; Swart and Fyfe 2012; Wilcox et al. 2012; Barnes and Polvani 2013; Bracegirdle et al. 2013; Lee et al. 2013; Swart et al. 2015; Simpson et al. 2016). However, whether these SO wind stress changes simulated and predicted in CMIP5 models are brought about by changes of the mean westerly winds, changes of wind variability, or both is unknown. The general role of wind fluctuations in determining the strength of SO wind stress in CMIP5 models is also unclear. The answers to these questions may prove useful for understanding the large spread in the model-simulated SO circulation and water masses under different scenarios (Wang et al. 2011; Meijers et al. 2012; Downes and Hogg 2013; Sallée et al., 2013a, 2013b; Wang 2013; Meijers 2014; Russell et al. 2018). In this study, we investigate for the first time the effects of wind fluctuations on the mean, seasonal cycle and trend of SO wind stress in CMIP5 models and compare them with results from two reanalysis products.

The paper is organized as follows. The CMIP5 models and reanalysis products chosen for this study are described in section 2, followed by an explanation of the analysis method used in section 3. In section 4, results of the effects of wind fluctuations at different time scales on

101 the mean, seasonal cycle and trend of the SO wind stresses in CMIP5 models are presented,
102 discussed and compared with those from the reanalysis products. Finally, conclusions and
103 discussion of implications of our results are provided in section 5.

104 **2. CMIP5 models and reanalysis products**

105 The CMIP5 models used in this study are listed in Table 1 together with model details such
106 as model resolution and whether stratosphere-resolving. CMIP5 models provide monthly-
107 mean surface wind stresses and eighteen of them at the time of this study provide 6-hourly
108 10-m wind velocities. To quantify the contributions from wind fluctuations at different time
109 scales to the SO wind stress, we recalculate wind stresses with wind fluctuations from these
110 eighteen models with certain time scales included or excluded by using an approximate
111 formulation of the dependence on 10-m wind speed. Only model output from historical runs
112 (1960-2005) is assessed, since for future projection simulations (Representative
113 Concentration Pathways RCP4.5 and RCP8.5), six-hourly wind velocities are only provided
114 for two 20-year periods of 2026-2046 and 2081-2100, which are not long enough for
115 estimating the trend significance.

116 Results from the CMIP5 models are compared with two widely-used atmospheric
117 reanalysis products: Japanese 55-year Reanalysis (JRA-55; Kobayashi et al. 2015) and ERA-
118 Interim Reanalysis (ERA-Interim; Dee et al. 2011). The horizontal resolutions of JRA-55 and
119 ERA-Interim are T319 (~63 km) and T255 (~80 km), respectively. The strength of the SH
120 westerly jet from reanalysis data suffers large spurious trends prior to 1979 but this situation
121 is much improved after 1979, thanks to the assimilation of Television Infrared Observation
122 Satellite (TIROS) Operational Vertical Sounder data into the reanalysis model (Hines et al.
123 2000; Kistler et al. 2001; Marshall 2003). In addition, the ERA-Interim winds are only
124 provided from 1979. Therefore, we choose to compare CMIP5 model outputs from historical
125 runs and the two reanalysis products over their overlapping period of 1979-2005. Note that

126 the differences between the mean wind stresses in CMIP5 models over the period of 1979-
127 2005 and those of 1960-2005 are generally very small (not shown). However, neither the
128 trends of SO wind stress in CMIP5 models nor those in the two reanalysis products are
129 significant over the period of 1979-2005. For this reason, the trends of SO wind stress in
130 CMIP5 models are calculated over the longer period of 1960-2005 and are not compared with
131 those from reanalysis products whose trends are known to be spurious prior to 1979.

132 **3. Methods**

133 Based on Monin–Obukhov similarity theory (MOST, Garratt 1994), bulk surface flux
134 parameterizations are used to estimate air-sea fluxes in CMIP5 models (Knutti et al. 2013;
135 Ma et al. 2015; Simpson et al. 2018) and bulk algorithms used to calculate surface
136 momentum and heat flux exchanges were provided in Fairall et al. (2003). Following Fairall
137 et al. (2003), the zonal surface wind stress in our study is calculated based on the bulk
138 formula $\tau_x = \rho_a c_d |U_{10}| u_{10}$, where τ_x is the surface zonal wind stress, $|U_{10}|$ is the 10-m wind
139 speed and u_{10} is the 10-m zonal wind velocity, ρ_a is air density at the sea surface (set to a
140 constant of $1.223\,\mathrm{kg/m^3}$), and c_d is the variable drag coefficient. Here c_d is set to the drag
141 coefficient in neutrally stable conditions from empirical functions $c_d^{1/2} = c_{dn}^{1/2} = \frac{\kappa}{\ln(z/z_0)}$ with
142 the MOST stability parameter $\zeta = 0$, where κ is von Karman's constant, z is the height of
143 wind measurement, z_0 is the roughness length for momentum. Following Smith (1988), the
144 roughness length is set to $z_0 = \frac{\alpha u_*^2}{g} + \frac{0.11\nu}{u_*}$, where α is the Charnock parameter, u_* is the
145 surface frictional velocity, gravitational acceleration g and kinematic viscosity ν are constants.
146 The Charnock parameter α varies with wind velocity and the surface frictional velocity is set
147 to $u_* = \frac{\kappa\sqrt{|U_{10}|^2 + u_g^2}}{\ln(z/z_0)}$ with a gustiness part u_g set to zero in neutrally stable conditions (Beljaars
148 1995; Fairall et al. 2003). As shown in Figure 1, the time-mean wind stresses calculated from
149 six-hourly winds of the eighteen CMIP5 models provide a reasonably close match to those

150 averaged from model output monthly-mean stresses. Differences in mean wind stress can be
151 attributed to neglecting atmosphere stability, waves and surface ocean currents, as well as
152 different Charnock parameter and gustiness used in our calculation of surface drag coefficient.
153 The methods used in this study to evaluate the effects of wind fluctuations at different time
154 scales on the SO wind stress are similar to those in Lin et al. (2018) but with some
155 modifications. It is worth pointing out that owing to the modulus function in the bulk formula
156 the contribution of wind fluctuations to the mean stress depends strongly on the presence of
157 the mean winds (Zhai 2013). For example, if the mean winds are ignored in the stress
158 calculation, the mean stress, to first-order approximation, vanishes regardless of the strength
159 of wind fluctuations. Here we follow Zhai (2013) and Lin et al. (2018) and quantify the
160 effects of including wind fluctuations at different time scales on the mean stress by including
161 /excluding these wind fluctuations in the stress calculation.
162 Different from Lin et al. (2018), we apply Lanczos low-pass-filter with 100 weights, rather
163 than the simple running-mean average, to the time series of 6-hourly CMIP5 and reanalysis
164 wind velocities at every model grid point to filter out wind fluctuations that last less than 2
165 days and 8 days. We have also tested the Butterworth filter and results are almost identical to
166 those using the Lanczos filter. Wind fluctuations on time scales of 2-8 days are calculated by
167 taking the difference between the 2-day low-pass filtered and 8-day low-pass filtered wind
168 fields. We then obtain the 2-8-day filtered winds by removing wind fluctuations on time
169 scales of 2-8 days from the original 6-hourly wind field (Table 2). Finally, we recalculate the
170 zonal wind stresses $\tau_{>2d}$, $\tau_{>8d}$, $\tau_{<2d\&>8d}$ and $\tau_{>yr}$ using 2-day filtered, 8-day filtered, 2-8-
171 day filtered and annual-mean winds, respectively (Table 2), and compare them with the zonal
172 wind stress $\tau_{>6hr}$ calculated from the original 6-hourly winds ($\tau_{>6hr}$ - $\tau_{>2d}$, $\tau_{>6hr}$ -
173 $\tau_{>8d}$, $\tau_{>6hr}$-$\tau_{<2d\&>8d}$, $\tau_{>6hr}$-$\tau_{>yr}$) to quantify the influences of including wind fluctuations
174 on time scales of less than 2 days, less than 8 days, 2-8 days and less than a year in the stress

calculation. For example, since wind fluctuations on 6 hours to 2 days are excluded in the calculation of $\tau_{>2d}$, the difference between $\tau_{>6hr}$ and $\tau_{>2d}$ can be used to quantify the effect of including wind fluctuations on 6 hours to 2 days on the mean stress. Threshold time scales of 2 days and 8 days are chosen because atmospheric variability on time scales of 2-8 days is generally thought to be associated with synoptic weather systems and baroclinic storm activities (e.g., Trenberth 1991; Yin 2005).

In addition, we also calculate and compare mean kinetic energy (MKE) and eddy kinetic energy (EKE) associated with the SO 10-m winds in CMIP5 models and reanalysis products. MKE in each year ($MKE_{<yr}$) at every grid point is calculated from the annual-mean wind field, and EKE at every grid point is calculated from wind fluctuations on time scales of 6 hours to 2 days ($EKE_{<2d}$), 2 to 8 days (EKE_{2-8d}), 6 hours to 8 days ($EKE_{<8d}$), and 6 hours to 1 year ($EKE_{<yr}$), respectively (see Table 2 for the formulas). For example, $EKE_{<2d}$ is calculated using the difference between the 6-hourly and 2-day low-pass filtered wind fields. As such, $EKE_{<2d}$ represents kinetic energy associated with wind fluctuations on time scales of 6 hours to 2 days alone and does not include the nonlinear cross term between fluctuations on 6 hours to 2 days and those on 2 days to 1 year.

4. Results

4.1 Mean state

4.1.1 Mean wind and stress

Figure 2 shows the 1979-2005 time-mean and zonal-mean zonal wind velocities (dashed lines) and zonal wind stresses (solid lines) in the SO from the eighteen CMIP5 models and two reanalysis data. There are considerable differences among them. The peak zonal wind velocities vary from 5.3 m s^{-1} in GISS-E2-H to 7.3 m s^{-1} in MIROC4h and peak values of $\tau_{>6hr}$ (red lines) vary from less than 0.11 N m^{-2} in GISS-E2-H to over 0.19 N m^{-2} in MIROC4h (see also red dots in Fig. 3a). The multi-model mean (MMM) zonal wind velocity

and wind stress are smaller than those from two reanalysis products (Figs. 2s-u and Fig. 3a). A large spread is shown in the latitudes of peak zonal wind velocities and peak zonal wind stresses, ranging from ~45°S to ~55°S in CMIP5 models. On the other hand, the latitudes of peak zonal wind stress and peak zonal wind velocity in the same model are close to each other, except in MRI-CGCM3 and MRI-ESM1. These results are consistent with the findings of previous studies (e.g. Bracegirdle et al. 2013; Lee et al. 2013).

There is also an equatorward bias of about 2° in the latitudes of maximum MMM zonal wind velocity and $\tau_{>6hr}$, compared to those in JRA-55 and ERA-Interim (Figs. 2s-u). This equatorward bias in the position of climatological zonal-mean SO winds exists in most CMIP5 models (Swart and Fyfe 2012; Wilcox et al. 2012; Bracegirdle et al. 2013; Russell et al. 2018). Ceppi et al. (2012) have argued that this equatorward bias is due to surface temperature gradient anomalies induced by mid-latitude shortwave cloud forcing bias. High-top models with model tops at or above 1hpa are marked in bold in Table 1. On average the mean positions of peak zonal winds in high-top models and low-top models are 49°S and 51°S, respectively. The larger equatorward bias found in high-top models can be related to the different upper meridional temperature gradients in high-top and low-top models (Wilcox et al. 2012; Bracegirdle et al. 2013).

4.1.2 Contributions from wind fluctuations to mean stress

In all eighteen CMIP5 models (Fig. 2a-r), the magnitude of $\tau_{>6hr}$ (red lines) is significantly greater than that of $\tau_{>yr}$ (yellow-green lines), confirming that wind fluctuations are a large contribution to the mean zonal wind stress in the SO (Zhai 2013). This is to be expected given the large wind variability in this storm track region and the non-linear dependence of surface wind stress on surface wind velocity. The effect of including wind fluctuations on 6 hours to 8 days (red vs purple lines) in the stress calculation is found to be comparable to that of including fluctuations on 8 days to 1 year (purple vs yellow-

225 green lines) in all 18 models. This result implies that wind fluctuations on a relatively
226 narrow time scale range of 6 hours to 8 days make a disproportionately large contribution to
227 the magnitude of the mean stress. Furthermore, the effect of including wind fluctuations on 2
228 to 8 days on the mean stress (cyan to red lines) is greater than that from including wind
229 fluctuations on 6 hours to 2 days (green to red lines in Fig. 2). These conclusions from the
230 CMIP5 models are consistent with those from the reanalysis data (Fig. 2s-u).

231 Figure 3a shows a quantitative comparison of the peak values of the 1979-2005 time-mean
232 and zonal-mean $\tau_{>6hr}$ (red), $\tau_{>2d}$ (green), $\tau_{<2d\&>8d}$ (cyan), $\tau_{>8d}$ (purple) and $\tau_{>yr}$ (yellow-
233 green) from the eighteen CMIP5 models and two reanalysis products. Although the spread
234 among the CMIP5 models is large for wind stresses calculated from six-hourly and four
235 filtered 10-m wind fields, the overall effect of including wind fluctuations at different time
236 scales on the peak mean wind stress is qualitatively similar. Focusing on the comparison
237 between the MMM and reanalysis products, the peak values of $\tau_{>yr}$ (yellow-green) are 0.066
238 N/m^2, 0.071 N/m^2 and 0.073 N/m^2 for the MMM (dashed line), JRA-55 and ERA-Interim,
239 respectively, and those of $\tau_{>6hr}$(red) are 0.158 N/m^2, 0.176 N/m^2 and 0.170 N/m^2. The peak
240 value of MMM $\tau_{>yr}$ is less than those in the two reanalysis products due to weaker mean
241 winds in CMIP5 models (Figs. 2s-u), while the smaller peak value of MMM $\tau_{>6hr}$ is due to
242 both weaker mean winds and weaker wind fluctuations (Fig. 3c). Stronger wind fluctuations
243 in JRA-55 lead to a greater strengthening effect on the mean stress via the nonlinear stress
244 law (see derivation in Zhai, 2013), which leads to a larger $\tau_{>6hr}$ in JRA-55 than in ERA-
245 interim (Fig. 3a and c).

246 Including wind fluctuations on time scales less than one year in the stress calculation is
247 found to increase the magnitude of peak zonal-mean zonal wind stress in the MMM, JRA-55
248 and ERA-Interim by about 145%, 148% and 135%, respectively (yellow-green line and dots
249 in Fig. 3b), with over 54% of the increase in the MMM and both reanalysis products being

contributed by wind fluctuations on time scales of 6 hours to 8 days (purple line and dots). Including wind fluctuations on time scales of 6 hours to 2 days and 2 to 8 days in the stress calculation act to increase the peak zonal-mean and time-mean wind stress in both MMM and two reanalysis products by around 15% and 35%, respectively (green and cyan lines and dots in Fig. 3b). Further dividing the CMIP5 models into different groups according to model resolution and whether stratosphere-resolving reveals no relationship between the effects of wind fluctuations on the mean stress and these model parameters/configurations (not shown).

4.1.3 Kinetic energy

The MKE and EKE are related to the large-scale mean wind field and wind fluctuations on much smaller scales, respectively. It is instructive to examine MKE and EKE in the CMIP5 models to understand the effect of mean wind and wind fluctuations at different time scales on the mean wind stress. Figure 4 shows the 1979-2005 time-mean and zonal-mean MKE and EKE, which are obtained by applying time average and zonal average to MKE and EKE calculated at every grid point. A few common features, consistent with results from the reanalysis products, emerge in all eighteen CMIP5 models. First, the zonal-mean $EKE_{<yr}$ is greater than the zonal-mean $MKE_{<yr}$ over the entire SO latitude range (35°S-65°S). Second, the meridional distribution of the zonal-mean $EKE_{<2d}$, EKE_{2-8d}, $EKE_{<8d}$ and $EKE_{<yr}$ is much broader and more uniform compared to $MKE_{<yr}$. The zonal-mean $EKE_{<yr}$ typically increases gradually southward to roughly 55°S-60°S before it drops more sharply poleward of that latitude band, except for MRI-CGCM3 and MRI-ESM1 where the zonal-mean $EKE_{<yr}$ increases monotonically southward and reaches values as high as 80 m^2 s^{-2} (yellow-green lines in Figs. 4q-r). As a consequence of this monotonic increase of $EKE_{<yr}$ with latitude, the distribution of $\tau_{>6hr}$ in these two models is skewed heavily southward (red lines in Figs. 2q-r). Further analysis shows that excluding results from MRI-CGCM3 and MRI-ESM1 leads to a noticeable decrease in the magnitude of the MMM $EKE_{<yr}$, particularly south of 55°S (grey

vs yellow-green in Fig. 4s). However, it is worth pointing out that the time and zonal averages of model output monthly mean wind stress from MRI-CGCM3 and MRI-ESM1 show no such large southward skewness (Figs. 1q and r). Third, EKE_{2-8d} is larger than $EKE_{<2d}$ in the SO (cyan vs green lines in Fig. 4), which explains why the effect of including wind fluctuations on time scales of 2 to 8 days on the mean stress is greater than that of including wind fluctuations on 6 hours to 2 days.

The peak values of the MMM $EKE_{<2d}$, EKE_{2-8d}, $EKE_{<8d}$ and $EKE_{<yr}$ are close to values from ERA-Interim although slightly smaller than those from JRA-55 (Fig. 3c). This is consistent with the results shown in Harvey et al. (2012), who demonstrated that the MMM storm tracks in CMIP5 models resemble the large-scale features of the storm tracks in the reanalysis data. Quantitatively, the MMM $EKE_{<2d}$, EKE_{2-8d}, and $EKE_{<8d}$ are found to account for about 17%, 40% and 57% of the MMM $EKE_{<yr}$ respectively, and these percentage contributions are similar to those in ERA-Interim and JRA-55 (Fig. 3d). The large percentage of $EKE_{<yr}$ accounted by $EKE_{<8d}$ explains why wind fluctuations on a relatively narrow time scale range of 6 hours to 8 days, when combined with the climatological mean wind, make a disproportionately large contribution to the strength of the mean stress via the nonlinear stress law (Fig. 3b).

4.2 Seasonal cycle

In this section we examine the effect of wind fluctuations on the seasonal cycle of SO wind stress in CMIP5 models. Despite considerable differences among the CMIP5 models in their simulated seasonal variations of zonal-mean winds and wind stresses, there are, again, a few common features (Fig. 5). In almost all eighteen CMIP5 models, the maximum zonal-mean zonal wind shifts to its most equatorward position in austral summer (dashed red), while the zonal-mean zonal wind becomes weaker and broader in austral winter (dashed black). This behavior is consistent with the northward expansion of the SH westerly wind belt and

300 decreased wind intensity in austral winter found by Lamy et al. (2010) and O'Kane et al.
301 (2017). In austral winter, the enhanced SO meridional temperature gradients increase the
302 available potential energy stored in the westerly winds (Gill 1982). This subsequently leads to
303 stronger atmospheric eddy activity and eddy-induced meridional momentum transport, which
304 modulates the strength and position of surface SO winds (Trenberth 1987; Lamy et al. 2010).
305 Larger EKE associated with enhanced eddy activities in austral winter can be found in Fig. 6.
306 In most models, the peak zonal-mean zonal wind stresses in austral spring and autumn are
307 much larger than those in summer and winter (Fig. 5). These features are also clearly seen in
308 the MMM plot (Fig. 5s) and are consistent with results from both reanalysis products (Figs.
309 5t-u). Interestingly, although the magnitude of the peak MMM zonal-mean wind in austral
310 summer is significantly greater than that in austral winter (by ~21%; red vs black dashed in
311 Fig. 5s), the peak MMM zonal-mean wind stress in austral summer is almost of the same
312 strength as that in austral winter (red vs black solid). In the two reanalysis products, the
313 magnitude of the peak zonal-mean wind in austral summer is greater than that in austral
314 winter, while the peak zonal-mean wind stress in austral summer is smaller than that in
315 austral winter (Fig. 5t-u; see also Lin et al. 2018). This paradox can be explained by the
316 pronounced seasonal cycle of the intensity of wind fluctuations in the SO. In all eighteen
317 CMIP5 models and both reanalysis products, the magnitude of wind fluctuations is the largest
318 in austral winter and smallest in austral summer (black and red dashed in Fig. 6), and EKE is
319 much greater than MKE in austral winter at all latitudes in the SO (black dashed vs solid).
320 Therefore, stronger wind variability in austral winter significantly enhances the winter-mean
321 zonal wind stress via the nonlinear stress law, which brings its peak strength to the same level
322 as that in austral summer, even though the peak zonal-mean wind in austral winter is
323 considerably weaker than that in austral summer.
324 Seasonal variability of the peak values of 1979-2005 monthly-mean and zonal-mean $\tau_{>6\mathrm{hr}}$

325 in the SO is dominated by a semiannual cycle in all eighteen CMIP5 models, despite the large
326 inter-model spread (Fig. 7a). The pattern of MMM wind stress (black solid), similar to those
327 from JRA-55 (blue solid) and ERA-Interim (red solid), is characterized by maximum values
328 in austral autumn (April) and spring (October) and minimum values in austral winter
329 (June/July) and summer (December). However, the magnitude of MMM wind stress is
330 somewhat smaller than those from JRA-55 and ERA-Interim. To understand where this
331 semiannual cycle of peak zonal-mean $\tau_{>6\mathrm{hr}}$ comes from, we examined seasonal variability of
332 the peak values of monthly-mean and zonal-mean MKE and EKE at the latitude of peak
333 monthly-mean and zonal-mean $\tau_{>6\mathrm{hr}}$ (Figs. 7b-c). It becomes clear that the semiannual cycle
334 of peak zonal-mean $\tau_{>6\mathrm{hr}}$ in the SO is associated with the semiannual cycle of the strength of
335 the mean wind. This semiannual oscillation of SO zonal-mean winds is a well-known
336 phenomenon and is caused by the variability of temperature gradients in the middle
337 troposphere (van Loon 1967). In contrast, the peak zonal-mean EKE in seventeen out of
338 eighteen CMIP5 models as well as in both reanalysis products shows a pronounced annual
339 cycle with its maximum in austral winter and minimum in austral summer (Fig. 7c). Figure 7
340 also shows the extremely large zonal-mean wind stress and EKE in MRI-CGCM3 and MRI-
341 ESM1 in months from July to October. The unrealistically large EKE in MRI-CGCM3 and
342 MRI-ESM1 in austral winter and spring (see also in Fig. 6q and r) contributes to the large and
343 heavily southward skewed wind stress in these two seasons (see also in Fig. 5q and r).

344 *4.3 Trend*

345 Wind stresses and kinetic energy at the position of peak annual-mean and zonal-mean $\tau_{>6\mathrm{hr}}$
346 are used for trend calculation. Only eleven out of the eighteen CMIP5 models show
347 significant wind stress ($\tau_{>6\mathrm{hr}}$) trends at <5% level by two-sided *t* test over the period of
348 1960-2005 (Table 3). The trends calculated from wind stresses (tauu) directly output by
349 CMIP5 models are also only significant in the same eleven models. Peak annual-mean and

zonal-mean SO wind stresses $\tau_{>6hr}$ (black), $\tau_{>yr}$ (grey) and kinetic energy $MKE_{<yr}$ (yellow-green), $EKE_{<yr}$ (green) from 1960 to 2005 in these eleven CMIP5 models are shown in Fig. 8 and their trends are given in Table 3. Not all these eleven models have significant trends in $\tau_{>yr}$ over this period; the trend of $\tau_{>yr}$ is not significant in GFDL-ESM2M. In the ten models where both the trends of $\tau_{>6hr}$ and $\tau_{>yr}$ are significant, the trends of $\tau_{>6hr}$ are, on average, over 50% greater than those of $\tau_{>yr}$, demonstrating the amplification effect of wind fluctuations on the calculated wind stress trend (Table 3). Furthermore, this amplification effect exists regardless of whether there is trend in the intensity of wind fluctuations. Due to the nonlinearity in the stress calculation, differences in the mean winds influence the effects that wind fluctuations have on the mean stress and its trend. In seven CMIP5 models, the peak annual-mean and zonal-mean SO wind stress ($\tau_{>6hr}$) exhibits a significant poleward shift of about 1 to 2 degrees over the period of 1960-2005 (not shown).

Consistent with the significant trends of $\tau_{>yr}$, the trends of $MKE_{<yr}$ are also significant in the same ten CMIP5 models, while the trend of $EKE_{<yr}$ is not significant in any of these ten models (Table 3). Therefore, the wind stress trends in these ten models are due to the strengthening of the mean winds, not the increase in storm activities. This is similar to the result derived from ERA-Interim reanalysis data over 1979-2016, that is, the strengthening SO wind stress in ERA-Interim is caused by the increasing strength of the mean westerly wind (Lin et al. 2018). In contrast, the trend of $EKE_{<yr}$ over the period of 1960-2005 is significant only in GFDL-ESM2M. However, the trends of $\tau_{>yr}$ and $MKE_{<yr}$ are not significant in this model (Table 3). Therefore, the significant trend of $\tau_{>6hr}$ in GFDL-ESM2M is caused by increased wind fluctuations, especially those on time scales less than eight days (significant trend of $EKE_{<8d}$ in Table 3), rather than the strengthening of the mean wind. The positive trends of $EKE_{<8d}$, $EKE_{<2d}$ and EKE_{2-8d} are significant in five, six and four models, respectively.

375 Based on the idealized model results of Munday and Zhai (2017), we expect the different
376 contributions of wind fluctuations to wind stress trends in GFDL-ESM2M and other models
377 to lead to considerable differences in the model-simulated SO overturning circulation and
378 water mass formation in response to forcing changes. For example, Downes and Hogg (2013)
379 found different strengths and changes of SO meridional overturning circulation in
380 ACCESS1.0, ACCESS1.3 and GFDL-ESM2M, all three of which share the same ocean
381 model but have different atmosphere, land, and sea ice components. Although the eddy-
382 induced overturning circulation in GFDL-ESM2M is weaker during the historical period
383 compared to ACCESS1.0 and ACCESS1.3, the increase in the strength of the eddy-driven
384 overturning in response to the RCP8.5 forcing is larger in GFDL-ESM2M (Figs. 8, 9 in
385 Downes and Hogg, 2013).
386 It is instructive to further examine the stress trends in different seasons in the eleven
387 models with significant wind stress trends over the period of 1960-2005 to distinguish the
388 contributions from different seasons. Note that the other seven CMIP5 models with no
389 significant trend over this period show either no significant trend in any season or only a
390 weak trend in DJF. Table 4 shows that no CMIP5 models have significant trends in $\tau_{>6hr}$ in
391 all four seasons over this period. The wind stress trends are found to be significant in austral
392 summer (DJF) in nine out of these eleven CMIP5 models, while in other seasons they are
393 significant only in a few models. Lin et al. (2018) also found that during 1979-2016 the trend
394 of SO wind stress in ERA-Interim is significant only in austral summer and autumn. The
395 strengthening trends are largest in austral summer in both reanalysis data and CMIP5 models
396 over the period of 1979-2010 have also been reported by Swart and Fyfe (2012). Previous
397 radiosonde and modeling studies show that the particularly large positive trend of SH
398 circumpolar westerly wind during austral summer is driven primarily by the large

399 tropospheric response to stratospheric ozone depletion in this season (e.g. Thompson and
400 Solomon 2002; Arblaster and Meehl 2006; Son et al. 2010; Thompson et al. 2011).

401 **5. Conclusion and Discussion**

402 The SH surface westerly wind stress, a major driver for SO circulation and water mass
403 transformation, is predicted to increase in the future. The recent modeling study by Munday
404 and Zhai (2017) shows that the sensitivity of SO circulation to wind stress changes depends
405 strongly on how these stress changes are brought about, i.e. by changes of the mean wind or
406 wind variability. Although the enhancement of wind stress due to the inclusion of wind
407 fluctuations is consistent across reanalysis products, the diagnosis of trends is not consistent
408 (Lin et al. 2018), which may have important implications not only for SO circulation but also
409 global ocean heat and carbon uptake. CMIP5 models are widely used to simulate historical
410 and predict future changes of the SH westerly winds, SO circulation and water mass
411 properties. However, the role of wind fluctuations in determining the strength of SO wind
412 stress in CMIP5 models has not been quantified before. In this study we have investigated the
413 effects of wind fluctuations on the mean, seasonal cycle and trend of SO wind stress in
414 eighteen CMIP5 models and compared them with results from two reanalysis products.
415 Despite considerable inter-model spread, a few conclusions appear to be robust and are
416 applicable to most, if not all, of the eighteen CMIP5 models:

417 - Wind fluctuations strongly enhance the strength of the mean wind stress in the SO. This
418 is expected given the large wind variability in this storm track region and the non-linear
419 dependence of surface wind stress on surface wind velocity. Including wind fluctuations
420 in the stress calculation is found to increase the magnitude of the peak MMM zonal-
421 mean wind stress by about 145%, with over 54% of the increase being contributed by
422 wind fluctuations on time scales of 6 hours to 8 days.

- There is a pronounced seasonal cycle in the intensity of wind fluctuations in the SO, being lowest in austral summer and highest in austral winter. Stronger wind fluctuations bring the peak strength of the zonal-mean wind stress in austral winter to the same level as that in austral summer, even though the magnitude of the zonal-mean wind in austral winter is considerably smaller than that in austral summer. The seasonal variability of the peak zonal-mean zonal wind and zonal wind stress is dominated by a semiannual cycle, characterized by maxima in austral autumn and spring and minima in austral winter and summer.
- The trends of SO $\tau_{>6hr}$ over the period of 1960-2005 are significant in eleven out of the eighteen CMIP5 models. Among the eleven models, the trend of atmospheric EKE is significant in GFDL-ESM2M but not in the other ten models, while the trend of $\tau_{>yr}$ is significant in the other ten models but not in GFDL-ESM2M. The significant stress trend in GFDL-ESM2M is due to the significant increase in the intensity of wind fluctuations, while the trends in the other ten models are due to the significant strengthening of the mean westerly wind. Due to the amplification effect of wind fluctuations, the trend of $\tau_{>6hr}$ is, on average, over 50% larger than the trend of $\tau_{>yr}$. Furthermore, the trends of $\tau_{>6hr}$ are found to be significant in austral summer in nine CMIP5 models, while in other seasons they are significant in much fewer models.

Perhaps not surprisingly, we have found a large spread in the simulated trends of SO wind and wind stress among the 18 CMIP5 models: 11 models with significant trends in wind stress, 10 with significant trends in mean wind and 1 with significant trend in wind fluctuations. These large trend discrepancies may have contributed to the differences seen in the simulated historical changes of SO circulation and property distributions in CMIP5 models (e.g. Wang et al. 2011; Meijers et al. 2012; Downes and Hogg 2013; Sallée et al., 2013a, 2013b; Wang 2013; Meijers 2014; Russell et al. 2018).

Two dynamical concepts ('eddy saturation' and 'eddy compensation') have been proposed in studies investigating the response of SO circulation to wind stress changes using eddy-resolving or eddy-permitting models in recent decades. Eddy saturation and eddy compensation refer to reduced sensitivity of Antarctic Circumpolar Current (ACC) transport and SO meridional overturning circulation to wind stress changes, respectively (Straub 1993; Viebahn and Eden 2010). In the eddy-saturation limit, the ACC transport is insensitive to the strengthened wind stress (Straub 1993; Hallberg and Gnanadesikan 2006; Munday et al. 2013). Differences in wind stress trends in CMIP5 models may not be crucial for modeled ACC transport as no significant relationship has been found between modeled ACC transport and the strength or position of SO wind stress (Wang et al. 2011; Meijers et al. 2012; Downes and Hogg 2013). Differences in the contributions of wind fluctuations to the stress trends among CMIP5 models, on the other hand, may lead to considerable differences in the simulated response of eddy-driven meridional overturning circulation as shown in Munday and Zhai (2017), thereby affecting the level of eddy compensation in the SO. The significant wind stress trend in GFDL-ESM2M is due to the increase in the intensity of wind fluctuations, while in ACCESS1.0 and ACCESS1.3 wind stress trends are due to the strengthening of the mean winds (Table 3). The increased storminess in GFDL-ESM2M could potentially enhance diabatic processes in the upper ocean and lead to a greater sensitivity of SO residual overturning circulation to wind stress changes in this model (Downes and Hogg 2013). Results from this study suggest that both the mean wind and wind fluctuations need to be better simulated in CMIP5 models in order to reduce the uncertainty in model-predicted SO response to forcing changes in the future.

Acknowledgments

This study is supported by the National Key R&D Program of China (2016YFA0601804).

XL is supported by the project (41906190) of National Natural Science Foundation of China and the Fundamental Research Funds for the Central Universities (2019B19014). XZ acknowledges support by a Royal Society International Exchanges Award (IE131025). ZW is supported by the project (41876220) of National Natural Science Foundation of China and the Fundamental Research Funds for the Central Universities (2017B04814, 2017B20714). DRM is supported by the Natural Environment Research Council (ORCHESTRA, grant number NE/N018095/1).

References

Arblaster, J. M., and G. A. Meehl, 2006: Contributions of external forcings to Southern Annular Mode trends. *J. Climate*, **19**, 2896–2905.

Barnes, E. A., and L. Polvani, 2013: Response of the midlatitude jets, and of their variability, to increased greenhouse gases in the CMIP5 models. *J. Climate*, **26**(18), 7117–7135.

Beljaars, A. C. M., 1995: The parametrization of surface fluxes in large-scale models under free convection. *Quarterly Journal of the Royal Meteorological Society*, **121**(522), 255–270.

Bracegirdle, T. J., and Coauthors, 2013: Assessment of surface winds over the Atlantic, Indian and Pacific Ocean sectors of the Southern Ocean in CMIP5 models: historical bias, forcing response, and state dependence. *J. Geophys. Res. Atmos.*, **118**, 547–562.

Ceppi, P., Y.-T. Hwang, D. M. Frierson, and D. L. Hartmann, 2012: Southern Hemisphere jet latitude biases in CMIP5 models linked to shortwave cloud forcing. *Geophys. Res. Lett.*, **39**, L19708.

Dee, D. P., and Coauthors, 2011: The ERA-Interim reanalysis: configuration and performance of the data assimilation system. *Quart. J. Roy. Meteor. Soc.*, **137**, 553–597.

498 Downes, S. M., and A. M. Hogg, 2013: Southern Ocean circulation and eddy compensation
499 in CMIP5 models. *J. Climate*, **26**(18), 7198–7220.
500 Fairall, C. W., E. F. Bradley, J. E. Hare, A. A. Grachev, and J. B. Edson, 2003: Bulk
501 parameterization of air–sea fluxes: Updates and verification for the COARE
502 algorithm. *J. Climate*, **16**(4), 571–591.
503 Garratt, J. R., 1994: The atmospheric boundary layer. Cambridge University Press,
504 Cambridge, 316.
505 Gent, P., 2016: Effects of southern hemisphere wind changes on the meridional overturning
506 circulation in models. *Ann. Rev. Mar. Sci.*, **8**, 79–94.
507 Gill, A. E., 1982: Atmosphere-Ocean Dynamics. *International Geophysics series*, W. L.
508 Donn, Ed., Academic Press.
509 Gille, S. T., 2008: Decadal-scale temperature trends in the Southern Hemisphere ocean. *J.*
510 *Climate*, **21**(18), 4749–4765, doi:10.1175/2008JCLI2131.
511 Hallberg, R., and A. Gnanadesikan, 2006: The role of eddies in determining the structure and
512 response of the wind-driven southern hemisphere overturning: Results from the
513 Modeling Eddies in the Southern Ocean (MESO) project. *J. Phys. Oceanogr.*, **36**,
514 2232–2252.
515 Harvey, B. J., L. C. Shaffrey, T. J. Woollings, G. Zappa, and K. I. Hodges, 2012: How large
516 are projected 21st century storm track changes?. *Geophys. Res. Lett.*, **39**, L18707.
517 Hines, K. M., D. H. Bromwich, and G. J. Marshall, 2000: Artificial surface pressure trends in
518 the NCEP–NCAR reanalysis over the Southern Ocean and Antarctica. *J. Climate*, **13**,
519 3940–3952.
520 Jones, J. M., and Coauthors, 2016: Assessing recent trends in high-latitude Southern
521 Hemisphere surface climate. *Nat. Clim. Change*, **6**(10), 917–926.
522 Kistler, R., and Coauthors, 2001: The NCEP–NCAR 50-Year Reanalysis: Monthly means

523 CD-ROM and documentation. *Bull. Amer. Meteor. Soc.*, **82**, 247–267.
524 Knutti, R., D. Masson, and A. Gettelman, 2013: Climate model genealogy: Generation
525 CMIP5 and how we got there. *Geophys. Res. Lett.*, **40**(6), 1194–1199.
526 Kobayashi, S., and Coauthors, 2015: The JRA-55 Reanalysis: General specifications and
527 basic characteristics. *J. Meteor. Soc. Japan*, **93**, 5–48.
528 Lamy, F., R. Kilian, H. W. Arz, J. P. Francois, J. Kaiser, M. Prange, and T. Steinke, 2010:
529 Holocene changes in the position and intensity of the southern westerly wind belt.
530 *Nat. Geosci.*, **3**(10), 695.
531 Langlais, C. E., S. R. Rintoul, and J. D. Zika, 2015: Sensitivity of Antarctic Circumpolar
532 Current transport and eddy activity to wind patterns in the Southern Ocean. *J. Phys.*
533 *Oceanogr.*, **45**(4), 1051–1067.
534 Large, W. G., J. C. McWilliams, and S. C. Doney, 1994: Oceanic vertical mixing: A review
535 and a model with a nonlocal boundary layer parameterization. *Rev. Geophys.*, **32**,
536 363–403.
537 Lee, T., D. E. Waliser, J. L. F. Li, F. W. Landerer, and M. M. Gierach, 2013: Evaluation of
538 CMIP3 and CMIP5 wind stress climatology using satellite measurements and
539 atmospheric reanalysis products. *J. Climate*, **26**(16), 5810–5826.
540 Le Quéré, C., and Coauthors, 2007: Saturation of the Southern Ocean CO2 sink due to recent
541 climate change. *Science*, **316**(5832), 1735–1738, doi:10.1126/science.1136188.
542 Lin, X., X. Zhai, Z. Wang, and D. Munday, 2018: Mean, variability and trend of Southern
543 Ocean wind stress: Role of wind fluctuations. *J. Climate,* **31**, 3557–3573.
544 Ma, Y., X. Zhou, D. Bi, Z. Sun, and A. C. Hirst, 2015: Improved air–sea flux algorithms in an
545 ocean–atmosphere coupled model for simulation of global ocean SST and its tropical
546 Pacific variability. *Climate Dyn.*, **44**(5–6), 1473–1485.
547 Marshall, G. J., 2003: Trends in the Southern Annular Mode from observations and

548 reanalyses. *J. Climate*, **16**, 4134–4143.
549 Marshall, J., and K. Speer, 2012: Closure of the meridional overturning circulation through
550 Southern Ocean upwelling. *Nat. Geosci.*, **5**(3), 171–180.
551 Meijers, A. J. S., E. Shuckburgh, N. Bruneau, J.-B. Sallée, T. J. Bracegirdle, and Z. Wang,
552 2012: Representation of the Antarctic Circumpolar Current in the CMIP5 climate
553 models and future changes under warming scenarios. *J. Geophys. Res. Oceans*, **117**,
554 C12008.
555 ——, 2014: The Southern Ocean in the Coupled Model Intercomparison Project phase 5.
556 *Phil. Trans. R. Soc. A*, **372**, 20130296.
557 Meredith, M. P., A. C. Naveira Garabato, A. M. Hogg and R. Farneti, 2012: Sensitivity of
558 the overturning circulation in the Southern Ocean to decadal changes in wind forcing.
559 *J. Climate*, **25**(1), 99–110.
560 Munday, D. R., H. L. Johnson, and D. P. Marshall, 2013: Eddy saturation of equilibrated
561 circumpolar currents. *J. Phys. Oceanogr.*, **43**, 507–532.
562 ——, and X. Zhai, 2017: The Impact of Atmospheric Storminess on the Sensitivity of
563 Southern Ocean Circulation to Wind Stress Changes. *Ocean Modell.*, **115**, 14–26.
564 O'Kane, T. J., D. P. Monselesan, and J. S. Risbey, 2017: A Multiscale Reexamination of the
565 Pacific–South American Pattern. *Mon. Weather Rev.*, **145**(1), 379–402.
566 Russell, J. L., and Coauthors, 2018: Metrics for the Evaluation of the Southern Ocean in
567 Coupled Climate Models and Earth System Models. *J. Geophys. Res. Oceans*, **123**,
568 3120–3143.
569 Sallée, J.-B., and Coauthors, 2013a: Assessment of Southern Ocean mixed layer depths in
570 CMIP5 models: Historical bias and forcing response. *J. Geophys. Res. Oceans*, **118**,
571 1845–1862.
572 ——, and Coauthors, 2013b: Assessment of Southern Ocean water mass circulation and

characteristics in CMIP5 models: Historical bias and forcing response. *J. Geophys. Res. Oceans*, **118**, 1830–1844.

Simpson, I. R., and L. M. Polvani, 2016: Revisiting the relationship between jet position, forced response, and annular mode variability in the southern midlatitudes. *Geophys. Res. Lett.*, **43**, 2896–2903.

Simpson, I. R., J. T. Bacmeister, I. Sandu, and M. J. Rodwell, 2018: Why Do Modeled and Observed Surface Wind Stress Climatologies Differ in the Trade Wind Regions?. *J. Climate*, **31**(2), 491–513.

Smith, S. D., 1988: Coefficients for sea surface wind stress, heat flux, and wind profiles as a function of wind speed and temperature. *J. Geophys. Res.*, **93**, 15467–15472.

Son, S.-W., and Coauthors, 2010: Impact of stratospheric ozone on Southern Hemisphere circulation change: A multimodel assessment. *J. Geophys. Res.*, **115**, D00M07, doi:10.1029/2010JD014271.

Straub, D. N., 1993: On the transport and angular momentum balance of channel models of the Antarctic Circumpolar Current. *J. Phys. Oceanogr.*, **23**, 776-782.

Swart, N. C., and J. C. Fyfe, 2012: Observed and simulated changes in the Southern Hemisphere surface westerly wind-stress. *Geophys. Res. Lett.*, **39**, L16711.

——, ——, N. Gillett, and G. J. Marshall, 2015: Comparing trends in the southern annular mode and surface westerly jet. *J. Climate*, **28**(22), 8840–8859.

Thompson, D. W. J., and S. Solomon, 2002: Interpretation of recent Southern Hemisphere climate change. *Science*, **296**, 895–899.

——, ——, P. J. Kushner, M. H. England, K. M. Grise, and D. J. Karoly, 2011: Signatures of the Antarctic ozone hole in Southern Hemisphere surface climate change. *Nat. Geosci.*, **4**, 741–749.

Trenberth, K. E., 1987: The role of eddies in maintaining the Westerlies in the Southern

598 Hemisphere winter. *J. Atmos. Sci.*, **44**, 1498–1508.
599 ——, 1991: Storm tracks in the Southern Hemisphere. *J. Atmos. Sci.*, **48**(19), 2159–2178.
600 van Loon, H., 1967: The half-yearly oscillations in middle and high southern latitudes and
601 the coreless winter. *J. Atmos. Sci.*, **24**(5), 472–486.
602 Viebahn, J., and C. Eden, 2010: Towards the impact of eddies on the response of the Southern
603 Ocean to climate change. *Ocean Modell.*, **34**(3), 150–165.
604 Wang, Z., 2013: On the response of Southern Hemisphere subpolar gyres to climate change
605 in coupled climate models. *J. Geophys. Res. Oceans*, **118**, 1070–1086.
606 ——, T. Kuhlbrodt, and M. P. Meredith, 2011: On the response of the Antarctic Circumpolar
607 Current transport to climate change in coupled climate models. *J. Geophys. Res.*
608 *Oceans*, **116**(C8).
609 ——, X. Zhang, Z. Guan, B. Sun, X. Yang, and C. Liu, 2015: An atmospheric origin of
610 the multi-decadal bipolar seesaw. *Scientific Reports*, **5**, 8909.
611 ——, Y. Wu, X. Lin, C. Liu, Z. Xie, 2017: Impacts of open-ocean deep convection in the
612 Weddell Sea on coastal and bottom water temperature. *Climate Dyn.*, **48**, 2967–2981,
613 doi:10.1007/s00382-016-3244-y.
614 Wilcox, L. J., A. J. Charlton-Perez, and L. J. Gray, 2012: Trends in Austral jet position in
615 ensembles of high− and low−top CMIP5 models. *J. Geophys. Res. Atmos.*, **117**,
616 D13115.
617 Wu, Y., X. Zhai, and Z. Wang, 2016: Impact of synoptic atmospheric forcing on the
618 mean ocean circulation. *J. Climate*, **29**(16), 5709–5724.
619 Yin, J. H., 2005: A consistent poleward shift of the storm tracks in simulations of 21st century
620 climate. *Geophys. Res. Lett.*, **32**, L18701.
621 Zhai, X., 2013: On the wind mechanical forcing of the ocean general circulation. *J. Geophys.*
622 *Res. Oceans*, **118**(12), 6561–6577.

——, and C. Wunsch, 2013: On the variability of wind power input to the oceans with a focus on the subpolar North Atlantic. *J. Climate*, **26**, 3892-3903.

——, H. L. Johnson, D. P. Marshall, and C. Wunsch, 2012: On the wind power input to the ocean general circulation. *J. Phys. Oceanogr.*, **42**, 1357–1365.

Zika, J. D., and Coauthors, 2013a: Vertical eddy fluxes in the Southern Ocean. *J. Phys. Oceanogr.*, **43**, 941–955.

——, J. Le Sommer, C. O. Dufour, A. Naveira-Garabato, and A. Blaker, 2013b: Acceleration of the Antarctic Circumpolar Current by wind stress along the coast of Antarctica. *J. Phys. Oceanogr.*, **43**, 2772–2784.

List of Tables

1. Details of CMIP5 models selected in this study. Models resolving the stratosphere well with model tops at or above 1hpa are defined as high-top models (in bold).
2. List of variables and formulas used in this study. The variables are defined in the similar way as in Lin et al. (2018), so the following text is derived from there with some minor changes. The Lanczos low-pass-filter is applied to the time series of 6-hourly wind velocities. Overbars "$\overline{\_}^{\mathrm{yr}}$", "$\overline{\_}^{\mathrm{2d}}$", "$\overline{\_}^{\mathrm{8d}}$" and "$\overline{\_}^{\mathrm{2-8d}}$" represent annual mean, 2-day low-pass filtered, 8-day low-pass filtered, and 2-8-day filtered winds, respectively, and superscript "6hr" indicates 6-hourly winds. Wind fluctuations on time scales of 2-8 days are removed from the 6-hourly wind fields to obtain the 2-8-day filtered winds, i.e., $\overline{u_{10}}^{2-8d} = u_{10}^{6hr} - (\overline{u_{10}}^{2d} - \overline{u_{10}}^{8d})$ and $\overline{v_{10}}^{2-8d} = v_{10}^{6hr} - (\overline{v_{10}}^{2d} - \overline{v_{10}}^{8d})$, respectively. The 2-8-day filtered wind speed is then calculated from $\left|\overline{U_{10}}^{2-8d}\right| = \sqrt{(\overline{u_{10}}^{2-8d})^2 + (\overline{v_{10}}^{2-8d})^2}$.
3. Significant trends of SO wind stresses (10^{-4} N m^{-2} yr^{-1}) in eleven CMIP5 models over the period of 1960-2005 calculated from model output wind stress (tauu) and $\tau_{>6hr}$, as well as trends of $\tau_{>yr}$ (10^{-4} N m^{-2} yr^{-1}) and kinetic energy (10^{-2} m^2 s^{-2} yr^{-1}) in these eleven models. Trends not significant at <5% level by two-sided *t* test are marked with "/".
4. Seasonal trends of SO wind stress (10^{-4} N m^{-2} yr^{-1}) over the period of 1960-2005 from eleven CMIP5 models in Table 3. Trends not significant at <5% level by two-sided *t* test are marked with "/". "DJF", "MAM", "JJA" and "SON" represent austral summer, autumn, winter and spring, respectively.

672 Table 1. Details of CMIP5 models selected in this study. Models resolving the stratosphere
673 well with model tops at or above 1hpa are defined as high-top models (in bold).

Model Name	Institute	Horizontal Resolution (Degree Longitude* Degree Latitude)	Vertical Levels	Model Top
1. ACCESS 1.0	CSIRO-BOM (Australia)	1.875 * 1.25	38	4 hPa
2. ACCESS 1.3	CSIRO-BOM (Australia)	1.875 * 1.25	38	4 hPa
3. CMCC-CM	CMCC (Italy)	0.75 * 0.75	31	10 hPa
4. CNRM-CM5	CNRM-CERFACS (France)	1.41 * 1.41	31	10 hPa
5. GFDL-CM3	NOAA GFDL (USA)	2.5 * 2.0	48	**0.01 hPa**
6. GFDL-ESM2G	NOAA GFDL (USA)	2.5 * 2.0	24	3 hPa
7. GFDL-ESM2M	NOAA GFDL (USA)	2.5 * 2.0	24	3 hPa
8. GISS-E2-H	NASA GISS (USA)	2.5 * 2.0	40	**0.1 hPa**
9. GISS-E2-R	NASA GISS (USA)	2.5 * 2.0	40	**0.1 hPa**
10. HadGEM2-ES	Met office (UK)	1.875 * 1.25	38	4 hPa
11. IPSL-CM5A-LR	IPSL (France)	3.75 * 1.875	39	**0.04 hPa**
12. IPSL-CM5A-MR	IPSL (France)	2.5 * 1.26	39	**0.04 hPa**
13. MIROC-ESM	MIROC (Japan)	2.8 * 2.8	80	**0.0036 hPa**
14. MIROC-ESM-CHEM	MIROC (Japan)	2.8 * 2.8	80	**0.0036 hPa**
15. MIROC4h	MIROC (Japan)	0.56 * 0.56	56	2.3 hPa
16. MIROC5	MIROC (Japan)	1.41 * 1.41	40	3 hPa
17. MRI-CGCM3	MRI (Japan)	1.125 * 1.125	48	**0.01 hPa**
18. MRI-ESM1	MRI (Japan)	1.125 * 1.125	48	**0.01 hPa**

674
675
676
677

Table 2. List of variables and formulas used in this study. The variables are defined in the similar way as in Lin et al. (2018), so the following text is derived from there with some minor changes. The Lanczos low-pass-filter is applied to the time series of 6-hourly wind velocities. Overbars "$\overline{}^{\mathrm{yr}}$", "$\overline{}^{\mathrm{2d}}$", "$\overline{}^{\mathrm{8d}}$" and "$\overline{}^{\mathrm{2-8d}}$" represent annual mean, 2-day low-pass filtered, 8-day low-pass filtered, and 2-8-day filtered winds, respectively, and superscript "6hr" indicates 6-hourly winds. Wind fluctuations on time scales of 2-8 days are removed from the 6-hourly wind fields to obtain the 2-8-day filtered winds, i.e., $\overline{u_{10}}^{2-8d} = u_{10}^{6hr} - (\overline{u_{10}}^{2d} - \overline{u_{10}}^{8d})$ and $\overline{v_{10}}^{2-8d} = v_{10}^{6hr} - (\overline{v_{10}}^{2d} - \overline{v_{10}}^{8d})$, respectively. The 2-8-day filtered wind speed is then calculated from $\left|\overline{U_{10}}^{2-8d}\right| = \sqrt{(\overline{u_{10}}^{2-8d})^2 + (\overline{v_{10}}^{2-8d})^2}$.

Variable	Definition	Formula
$\boldsymbol{\tau_{>6hr}}$	Zonal wind stress calculated from 6-hourly winds	$\overline{\rho_a c_d \left\|U_{10}^{6hr}\right\| u_{10}^{6hr}}^{yr}$
$\boldsymbol{\tau_{>2d}}$	Zonal wind stress calculated from 2-day filtered winds	$\overline{\rho_a c_d \left\|\overline{U_{10}}^{2d}\right\| \overline{u_{10}}^{2d}}^{yr}$
$\boldsymbol{\tau_{>8d}}$	Zonal wind stress calculated from 8-day filtered winds	$\overline{\rho_a c_d \left\|\overline{U_{10}}^{8d}\right\| \overline{u_{10}}^{8d}}^{yr}$
$\boldsymbol{\tau_{<2d\&>8d}}$	Zonal wind stress calculated from 2-8-day filtered winds	$\overline{\rho_a c_d \left\|\overline{U_{10}}^{2-8d}\right\| \overline{u_{10}}^{2-8d}}^{yr}$
$\boldsymbol{\tau_{>yr}}$	Zonal wind stress calculated from annual-mean winds	$\overline{\rho_a c_d \left\|\overline{U_{10}}^{yr}\right\| \overline{u_{10}}^{yr}}^{yr}$
$\mathbf{MKE_{<yr}}$	Kinetic energy calculated from annual-mean winds	$\overline{\frac{(\overline{u_{10}}^{yr})^2 + (\overline{v_{10}}^{yr})^2}{2}}^{yr}$
$\mathbf{EKE_{<yr}}$	Kinetic energy calculated from wind fluctuations on time scales	$\overline{\frac{(u_{10}^{6hr} - \overline{u_{10}}^{yr})^2 + (v_{10}^{6hr} - \overline{v_{10}}^{yr})^2}{2}}^{yr}$

	of 6 hours to 1 year	
$\mathbf{EKE_{<2d}}$	Kinetic energy calculated from wind fluctuations on time scales of 6 hours to 2 days alone	$\overline{\frac{(u_{10}^{6hr} - \overline{u_{10}}^{2d})^2 + (v_{10}^{6hr} - \overline{v_{10}}^{2d})^2}{2}}^{yr}$
$\mathbf{EKE_{<8d}}$	Kinetic energy calculated from wind fluctuations on time scales of 6 hours to 8 days alone	$\overline{\frac{(u_{10}^{6hr} - \overline{u_{10}}^{8d})^2 + (v_{10}^{6hr} - \overline{v_{10}}^{8d})^2}{2}}^{yr}$
$\mathbf{EKE_{2-8d}}$	Kinetic energy calculated from wind fluctuations on time scales of 2 to 8 days alone	$\overline{\frac{(\overline{u_{10}}^{2d} - \overline{u_{10}}^{8d})^2 + (\overline{v_{10}}^{2d} - \overline{v_{10}}^{8d})^2}{2}}^{yr}$

Table 3. Significant trends of SO wind stresses (10^{-4} N m^{-2} yr^{-1}) in eleven CMIP5 models over the period of 1960-2005 calculated from model output wind stress (tauu) and $\tau_{>6hr}$, as well as trends of $\tau_{>yr}$ (10^{-4} N m^{-2} yr^{-1}) and kinetic energy (10^{-2} m^2 s^{-2} yr^{-1}) in these eleven models. Trends not significant at <5% level by two-sided *t* test are marked with "/".

Model Name	tauu	$\tau_{>6hr}$	$\tau_{>yr}$	$MKE_{<yr}$	$EKE_{<yr}$	$EKE_{<8d}$	$EKE_{<2d}$	EKE_{2-8d}
ACCESS 1.0	3.2	3.1	2.1	6.5	/	1.6	1.2	/
ACCESS 1.3	2.9	2.8	2.1	6.9	/	/	0.8	/
CMCC-CM	3.7	3.9	2.2	6.9	/	1.8	/	1.2
GFDL-CM3	2.9	3.8	2.6	8.3	/	/	/	/
GFDL-ESM2G	3.3	3.8	2.2	7.2	/	1.9	/	1.3
GFDL-ESM2M	2.4	2.8	/	/	2.8	2.1	1.0	1.1
GISS-E2-H	2.7	3.2	1.9	6.5	/	/	1.0	/
GISS-E2-R	3.4	2.9	1.7	5.8	/	1.9	0.9	1.0
IPSL-CM5A-LR	3.7	2.9	2.1	7.2	/	/	0.6	/
MIROC-ESM-CHEM	2.3	2.4	1.8	5.7	/	/	/	/
MRI-ESM1	3.1	4.6	2.1	7.1	/	/	/	/

715 Table 4. Seasonal trends of SO wind stress (10^{-4} N m^{-2} yr^{-1}) over the period of 1960-2005
716 from eleven CMIP5 models in Table 3. Trends not significant at <5% level by two-sided *t* test
717 are marked with "/". "DJF", "MAM", "JJA" and "SON" represent austral summer, autumn,
718 winter and spring, respectively.

Model Name	DJF	MAM	JJA	SON
ACCESS 1.0	5.0	/	/	/
ACCESS 1.3	/	/	/	3.5
CMCC-CM	/	/	8.0	7.0
GFDL-CM3	5.6	3.5	/	5.7
GFDL-ESM2G	4.9	5.5	/	/
GFDL-ESM2M	4.4	/	/	/
GISS-E2-H	5.2	/	/	/
GISS-E2-R	2.6	5.0	/	/
IPSL-CM5A-LR	3.0	3.4	/	/
MIROC-ESM-CHEM	3.1	/	/	/
MRI-ESM1	7.8	/	/	/

719
720
721
722
723
724
725
726
727

List of Figures

1. The 1979-2005 time-mean and zonal-mean zonal wind stresses from (a)-(r) the eighteen CMIP5 models (N m^{-2}) (blue: calculated using monthly mean wind stress data from the model output; red: calculated using $\tau_{>6hr}$ that is derived from the bulk formula and six-hourly winds).
2. The 1979-2005 time-mean and zonal-mean zonal wind velocities (dashed; m s^{-1}) and zonal wind stresses (solid; N m^{-2}) from (a)-(r) the eighteen CMIP5 models, (s) their multi-model mean, (t) JRA-55 and (u) ERA-Interim. Mean $\tau_{>6hr}$, $\tau_{>2d}$, $\tau_{<2d\&>8d}$, $\tau_{>8d}$ and $\tau_{>yr}$ are calculated from the 6-hourly, 2-day filtered, 8-day filtered, 2-8-day filtered, and annual-mean winds, respectively (see Table 2).
3. The peak values of 1979-2005 time-mean and zonal-mean (a) $\tau_{>6hr}$(red), $\tau_{>2d}$ (green), $\tau_{<2d\&>8d}$(cyan), $\tau_{>8d}$(purple) and $\tau_{>yr}$ (yellow-green) shown in Fig. 2 over the Southern Ocean (35°-65°S) from eighteen CMIP5 models and two reanalysis products; (b) Percentage increases in the peak value of the zonal-mean and time-mean wind stress when including in the stress calculation wind fluctuations on time scales less than a year $((\tau_{>6hr}-\tau_{>yr})/\tau_{>yr}$; yellow-green), and contributions from wind fluctuations on 6 hours to 2 days $((\tau_{>6hr}-\tau_{>2d})/(\tau_{>6hr}-\tau_{>yr})$; green), 2 to 8 days $((\tau_{>6hr}-\tau_{<2d\&>8d})/(\tau_{>6hr}-\tau_{>yr})$; cyan) and 6 hours to 8 days $((\tau_{>6hr}-\tau_{>8d})/(\tau_{>6hr}-\tau_{>yr})$; purple); (c) Same as (a) but for $MKE_{<yr}$ (black), $EKE_{<2d}$ (green), EKE_{2-8d} (cyan), $EKE_{<8d}$ (purple) and $EKE_{<yr}$ (yellow-green); (d) The ratios of $EKE_{<2d}/EKE_{<yr}$ (green), $EKE_{2-8d}/EKE_{<yr}$ (cyan) and $EKE_{<8d}/EKE_{<yr}$ (purple). The dash-dotted lines mark the corresponding multi-model mean values.
4. The 1979-2005 time-mean and zonal-mean mean kinetic energy (m^2 s^{-2}) and eddy kinetic energy (m^2 s^{-2}) from (a)-(r) the eighteen CMIP5 models, (s) their multi-model mean, (t)

JRA-55 and (u) ERA-Interim. Mean kinetic energy $MKE_{<yr}$ (black) at every grid point is calculated from the annual-mean winds in each year, and eddy kinetic energy $EKE_{<2d}$(green), EKE_{2-8d}(cyan), $EKE_{<8d}$ (purple) and $EKE_{<yr}$ (yellow-green) at every grid point are calculated from wind fluctuations on time scales of 6 hours to 2 days, 2 to 8 days, 6 hours to 8 days, and 6 hours to 1 year, respectively (see Table 2). The maximum values of vertical axis in MRI-CGCM3 (q) and MRI-ESM1 (r) are adjusted to 80m^2 s^{-2}. The grey line in (s) is the multi-model mean without MRI-CGCM3 and MRI-ESM1.

5. The 1979-2005 seasonal-mean and zonal-mean zonal wind velocities (dashed; m s^{-1}) and zonal wind stresses (solid; N m^{-2}) from (a)-(r) the eighteen CMIP5 models, (s) their multi-model mean, (t) JRA-55 and (u) ERA-Interim.
6. The 1979-2005 seasonal-mean and zonal-mean mean kinetic energy (solid; m^2 s^{-2}) and eddy kinetic energy (dashed; m^2 s^{-2}) from (a)-(r) the eighteen CMIP5 models, (s) their multi-model mean, (t) JRA-55 and (u) ERA-Interim.
7. Seasonal variability of (a) the peak values of 1979-2005 monthly-mean and zonal-mean zonal wind stress $\tau_{>6hr}$ (N m^{-2}), (b) mean kinetic energy (m^2 s^{-2}) and (c) eddy kinetic energy (m^2 s^{-2}) over the SO (35°-65°S) from the eighteen CMIP5 models (dashed), their multi-model mean (solid black), JRA-55 (solid blue) and ERA-Interim (solid red).
8. Peak annual-mean and zonal-mean SO wind stresses $\tau_{>6hr}$ (black), $\tau_{>yr}$ (grey, N m^{-2}) and kinetic energy $MKE_{<yr}$ (yellow-green), $EKE_{<yr}$ (green, m^2 s^{-2}) at the position of peak annual-mean and zonal-mean $\tau_{>6hr}$ from 1960 to 2005 in the eleven CMIP5 models. The dash-dotted lines represent corresponding trends. Trends of $\tau_{>6hr}$ are significant in all eleven models, trends of $\tau_{>yr}$ and $MKE_{<yr}$ are significant in all eleven models except for GFDL-ESM2M, and the trend of $EKE_{<yr}$ is only significant in GFDL-ESM2M (see Table 3).

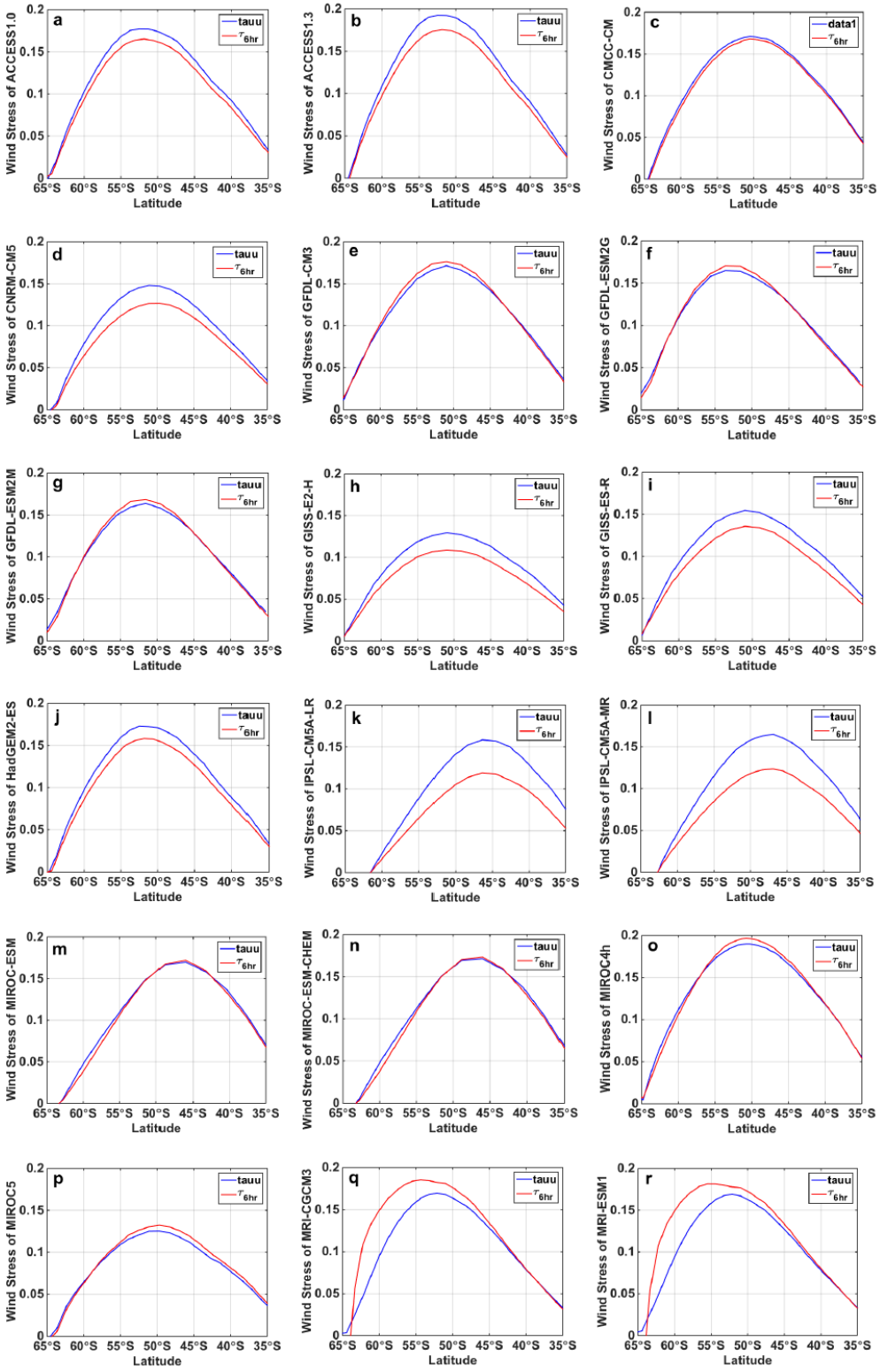

777

778 FIG. 1. The 1979-2005 time-mean and zonal-mean zonal wind stresses from (a)-(r) the
779 eighteen CMIP5 models (N m^{-2}) (blue: calculated using monthly mean wind stress data from
780 the model output; red: calculated using $\tau_{>6hr}$ that is derived from the bulk formula and six-
781 hourly winds).

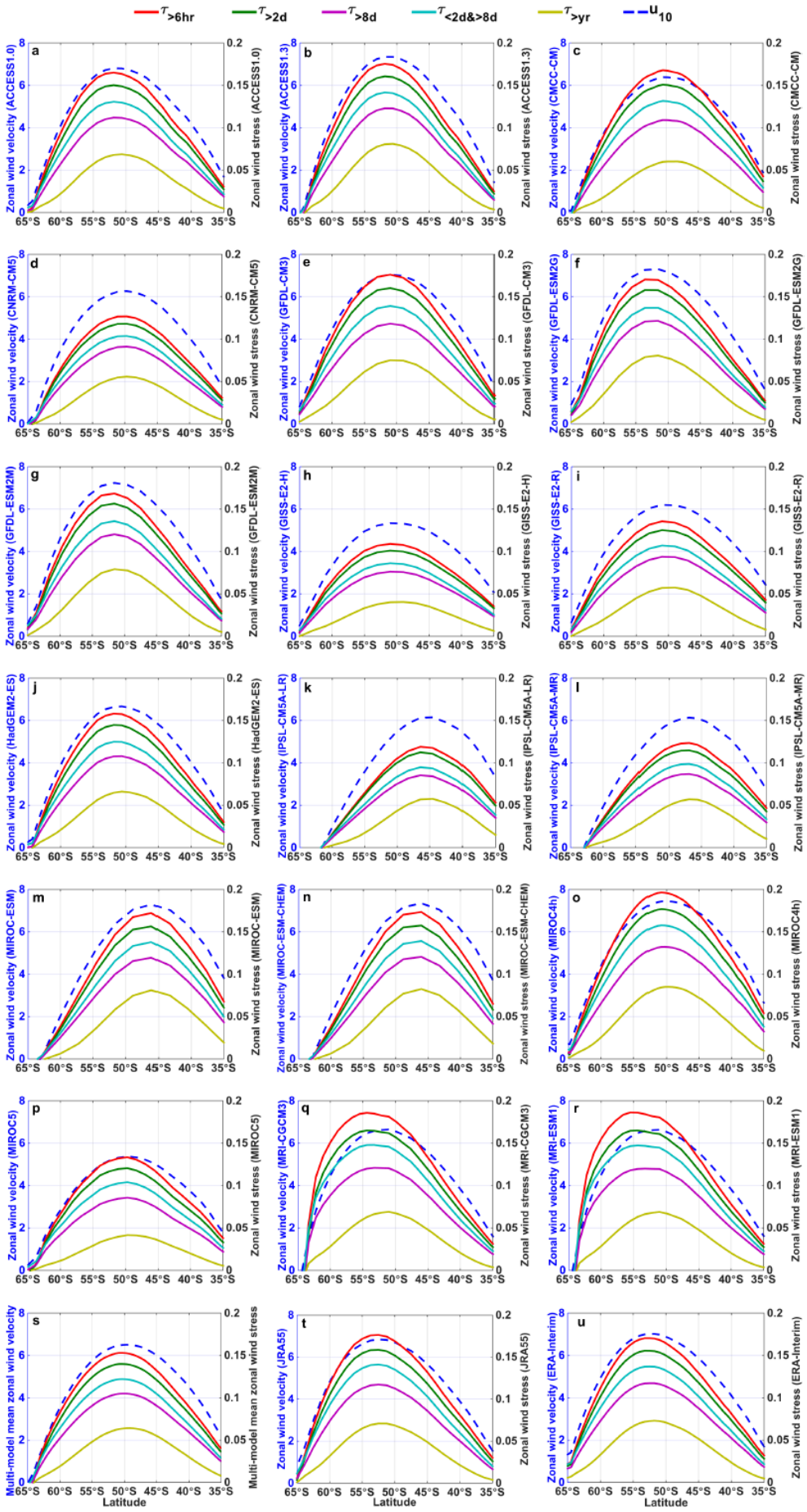
τ>6hr
τ>2d
τ>8d
τ<2d&>8d
τ>yr
u10
a
b
c
d
e
f
g
h
i
j
k
l
m
n
o
p
q
r
s
t
u
Zonal wind velocity (ACCESS1.0)
Zonal wind stress (ACCESS1.0)
Zonal wind velocity (ACCESS1.3)
Zonal wind stress (ACCESS1.3)
Zonal wind velocity (CMCC-CM)
Zonal wind stress (CMCC-CM)
Zonal wind velocity (CNRM-CM5)
Zonal wind stress (CNRM-CM5)
Zonal wind velocity (GFDL-CM3)
Zonal wind stress (GFDL-CM3)
Zonal wind velocity (GFDL-ESM2G)
Zonal wind stress (GFDL-ESM2G)
Zonal wind velocity (GFDL-ESM2M)
Zonal wind stress (GFDL-ESM2M)
Zonal wind velocity (GISS-E2-H)
Zonal wind stress (GISS-E2-H)
Zonal wind velocity (GISS-E2-R)
Zonal wind stress (GISS-E2-R)
Zonal wind velocity (HadGEM2-ES)
Zonal wind stress (HadGEM2-ES)
Zonal wind velocity (IPSL-CM5A-LR)
Zonal wind stress (IPSL-CM5A-LR)
Zonal wind velocity (IPSL-CM5A-MR)
Zonal wind stress (IPSL-CM5A-MR)
Zonal wind velocity (MIROC-ESM)
Zonal wind stress (MIROC-ESM)
Zonal wind velocity (MIROC-ESM-CHEM)
Zonal wind stress (MIROC-ESM-CHEM)
Zonal wind velocity (MIROC4h)
Zonal wind stress (MIROC4h)
Zonal wind velocity (MIROC5)
Zonal wind stress (MIROC5)
Zonal wind velocity (MRI-CGCM3)
Zonal wind stress (MRI-CGCM3)
Zonal wind velocity (MRI-ESM1)
Zonal wind stress (MRI-ESM1)
Multi-model mean zonal wind velocity
Multi-model mean zonal wind stress
Zonal wind velocity (JRA55)
Zonal wind stress (JRA55)
Zonal wind velocity (ERA-Interim)
Zonal wind stress (ERA-Interim)
65°S 60°S 55°S 50°S 45°S 40°S 35°S
Latitude
0 2 4 6 8
0 0.05 0.1 0.15 0.2

782

783 FIG. 2. The 1979-2005 time-mean and zonal-mean zonal wind velocities (dashed; m s^{-1}) and
784 zonal wind stresses (solid; N m^{-2}) from (a)-(r) the eighteen CMIP5 models, (s) their multi-
785 model mean, (t) JRA-55 and (u) ERA-Interim. Mean $\tau_{>6hr}$, $\tau_{>2d}$, $\tau_{<2d\&>8d}$, $\tau_{>8d}$ and $\tau_{>yr}$
786 are calculated from the 6-hourly, 2-day filtered, 8-day filtered, 2-8-day filtered, and annual-
787 mean winds, respectively (see Table 2).
788

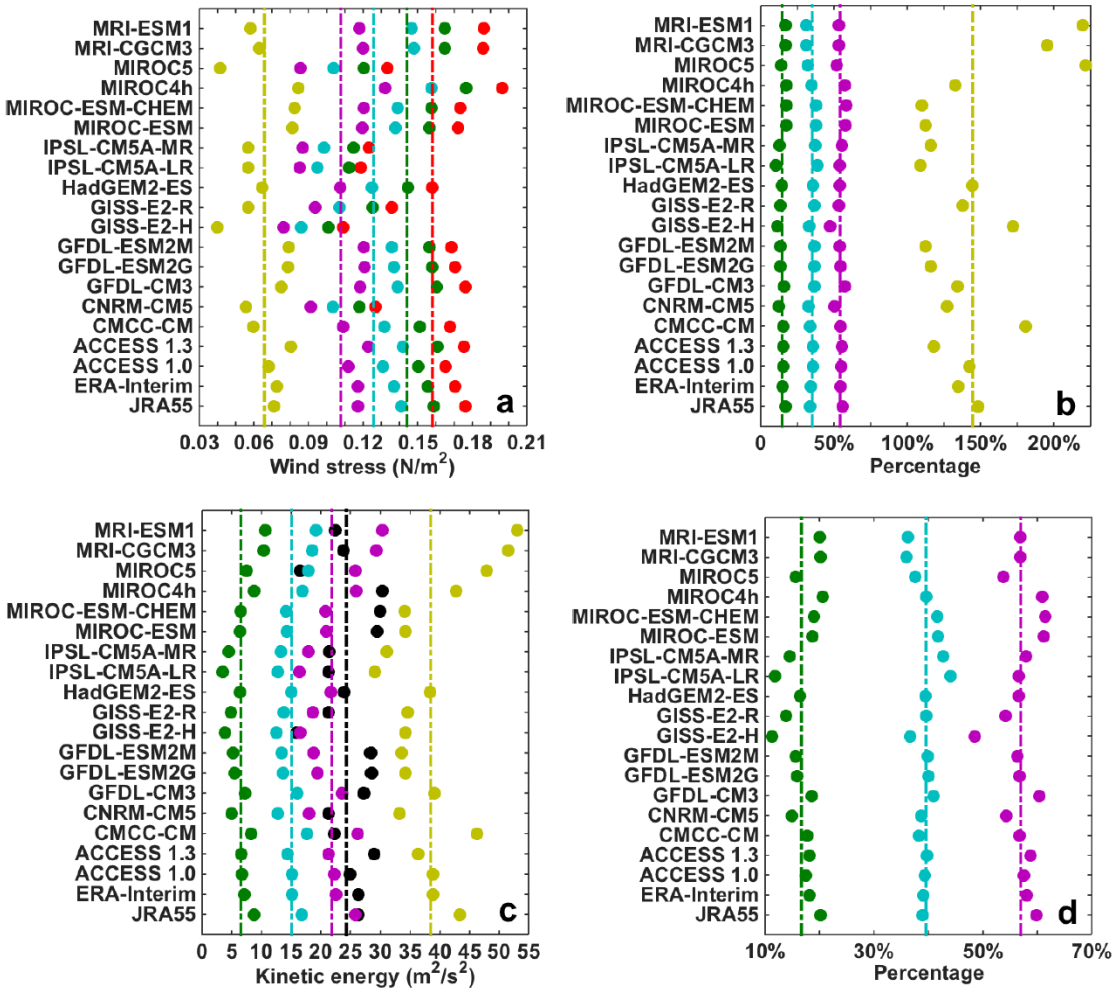

789

790 FIG. 3. The peak values of 1979-2005 time-mean and zonal-mean (a) $\tau_{>6hr}$ (red),
791 $\tau_{>2d}$ (green), $\tau_{<2d\&>8d}$(cyan), $\tau_{>8d}$(purple) and $\tau_{>yr}$ (yellow-green) shown in Fig. 2 over the
792 Southern Ocean (35º-65ºS) from eighteen CMIP5 models and two reanalysis products; (b)
793 Percentage increases in the peak value of the zonal-mean and time-mean wind stress when
794 including in the stress calculation wind fluctuations on time scales less than a year (($\tau_{>6hr}$-

795 $\tau_{>yr}$)/ $\tau_{>yr}$; yellow-green), and contributions from wind fluctuations on 6 hours to 2 days
796 (($\tau_{>6hr}$-$\tau_{>2d}$)/ ($\tau_{>6hr}$-$\tau_{>yr}$); green), 2 to 8 days (($\tau_{>6hr}$-$\tau_{<2d\&>8d}$)/ ($\tau_{>6hr}$-$\tau_{>yr}$); cyan) and
797 6 hours to 8 days (($\tau_{>6hr}$ - $\tau_{>8d}$)/ ($\tau_{>6hr}$ - $\tau_{>yr}$); purple); (c) Same as (a) but for
798 $MKE_{<yr}$ (black), $EKE_{<2d}$ (green), EKE_{2-8d} (cyan), $EKE_{<8d}$ (purple) and $EKE_{<yr}$ (yellow-
799 green); (d) The ratios of $EKE_{<2d}/EKE_{<yr}$ (green), $EKE_{2-8d}/EKE_{<yr}$ (cyan) and $EKE_{<8d}/$
800 $EKE_{<yr}$ (purple). The dash-dotted lines mark the corresponding multi-model mean values.

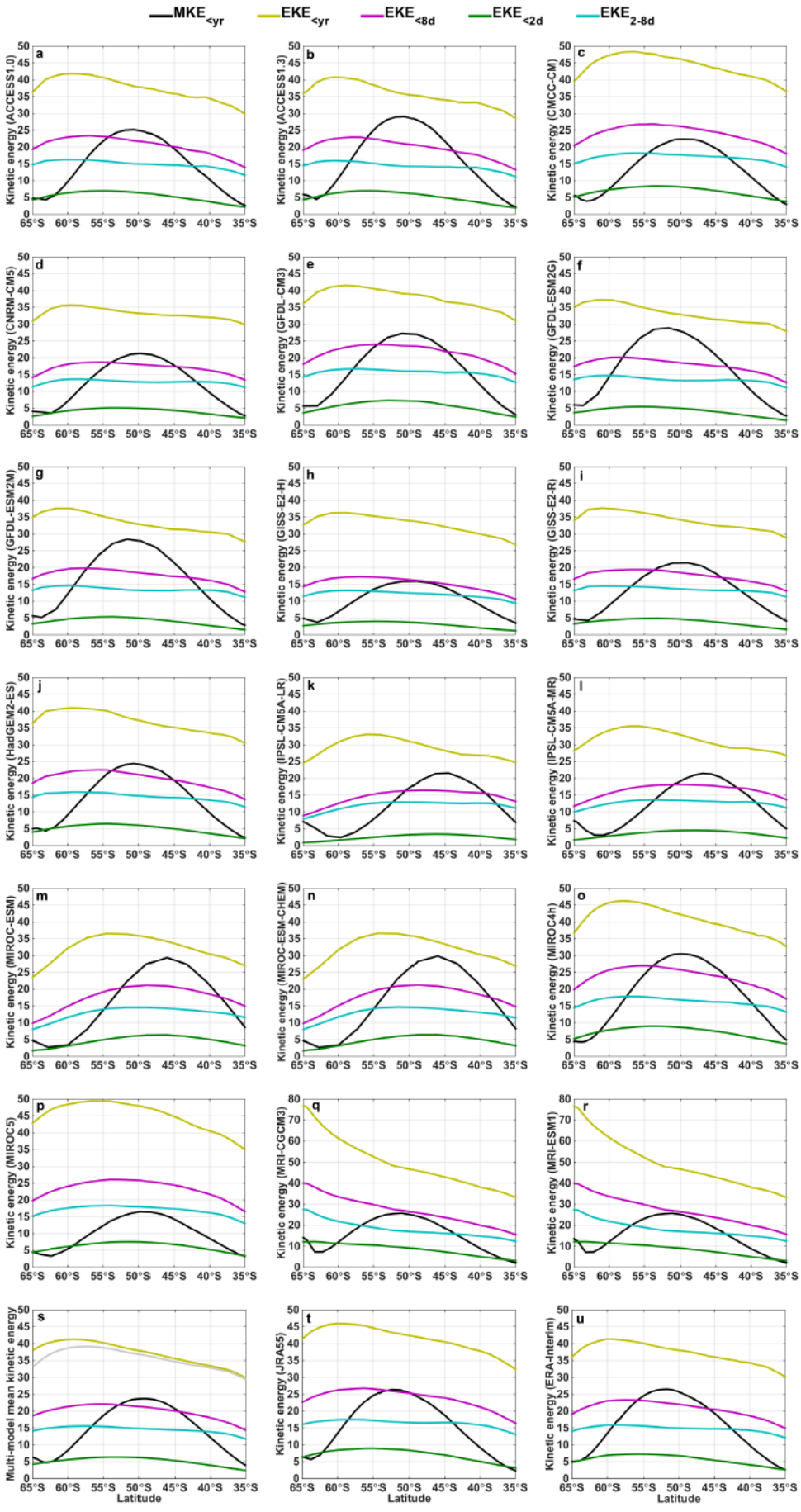
MKE<yr
EKE<yr
EKE<8d
EKE<2d
EKE2-8d
a
Kinetic energy (ACCESS1.0)
b
Kinetic energy (ACCESS1.3)
c
Kinetic energy (CMCC-CM)
d
Kinetic energy (CNRM-CM5)
e
Kinetic energy (GFDL-CM3)
f
Kinetic energy (GFDL-ESM2G)
g
Kinetic energy (GFDL-ESM2M)
h
Kinetic energy (GISS-E2-H)
i
Kinetic energy (GISS-E2-R)
j
Kinetic energy (HadGEM2-ES)
k
Kinetic energy (IPSL-CM5A-LR)
l
Kinetic energy (IPSL-CM5A-MR)
m
Kinetic energy (MIROC-ESM)
n
Kinetic energy (MIROC-ESM-CHEM)
o
Kinetic energy (MIROC4h)
p
Kinetic energy (MIROC5)
q
Kinetic energy (MRI-CGCM3)
r
Kinetic energy (MRI-ESM1)
s
Multi-model mean kinetic energy
t
Kinetic energy (JRA55)
u
Kinetic energy (ERA-Interim)
65°S 60°S 55°S 50°S 45°S 40°S 35°S
Latitude

801

802 FIG. 4. The 1979-2005 time-mean and zonal-mean mean kinetic energy (m^2 s^{-2}) and eddy
803 kinetic energy (m^2 s^{-2}) from (a)-(r) the eighteen CMIP5 models, (s) their multi-model mean, (t)
804 JRA-55 and (u) ERA-Interim. Mean kinetic energy $MKE_{<yr}$ (black) at every grid point is
805 calculated from the annual-mean winds in each year, and eddy kinetic energy $EKE_{<2d}$(green),
806 EKE_{2-8d} (cyan), $EKE_{<8d}$ (purple) and $EKE_{<yr}$ (yellow-green) at every grid point are
807 calculated from wind fluctuations on time scales of 6 hours to 2 days, 2 to 8 days, 6 hours to
808 8 days, and 6 hours to 1 year, respectively (see Table 2). The maximum values of vertical axis
809 in MRI-CGCM3 (q) and MRI-ESM1 (r) are adjusted to 80m^2 s^{-2}. The grey line in (s) is the
810 multi-model mean without MRI-CGCM3 and MRI-ESM1.

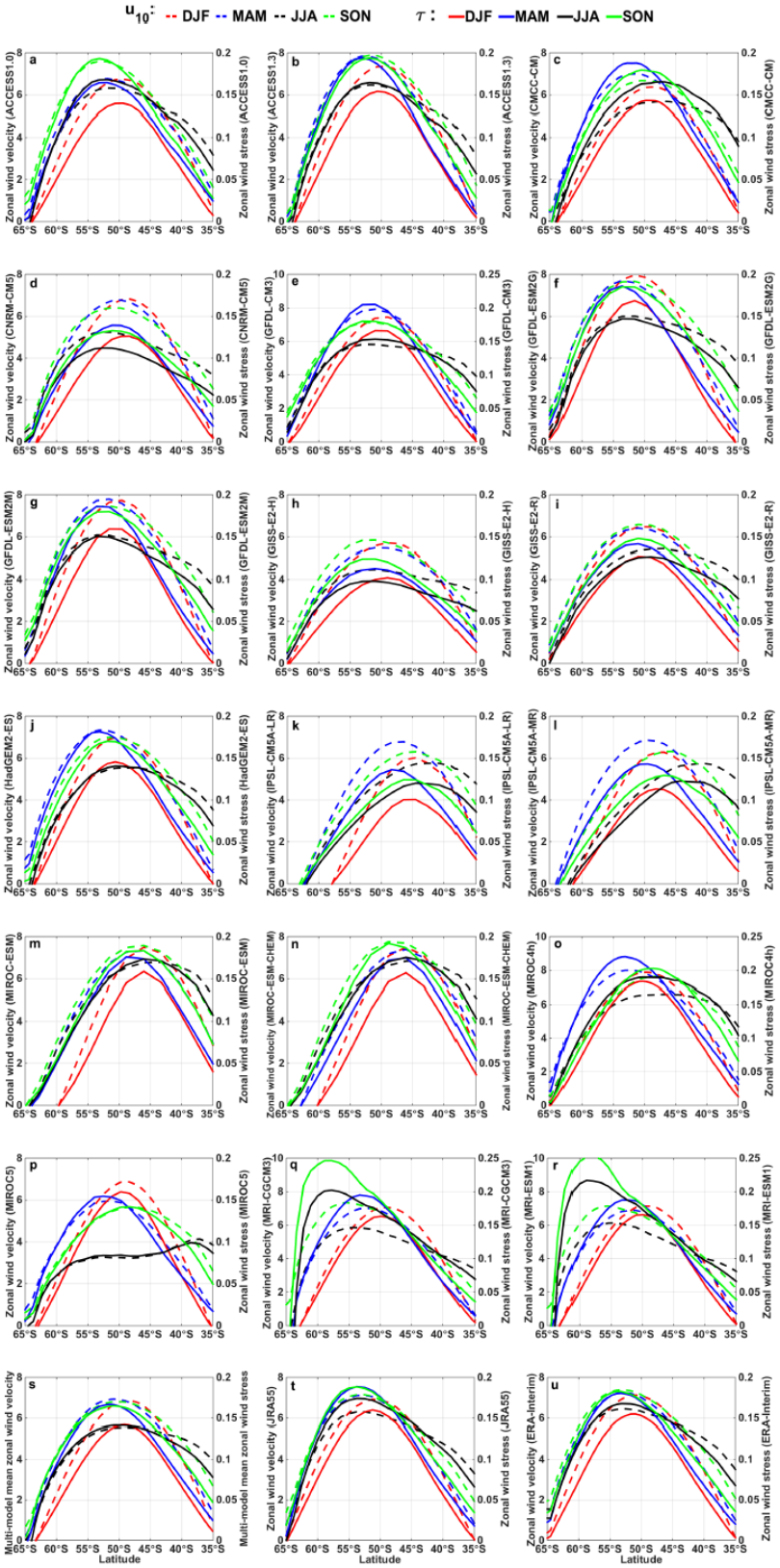

811

812 FIG. 5. The 1979-2005 seasonal-mean and zonal-mean zonal wind velocities (dashed; m s^{-1})
813 and zonal wind stresses (solid; N m^{-2}) from (a)-(r) the eighteen CMIP5 models, (s) their
814 multi-model mean, (t) JRA-55 and (u) ERA-Interim.

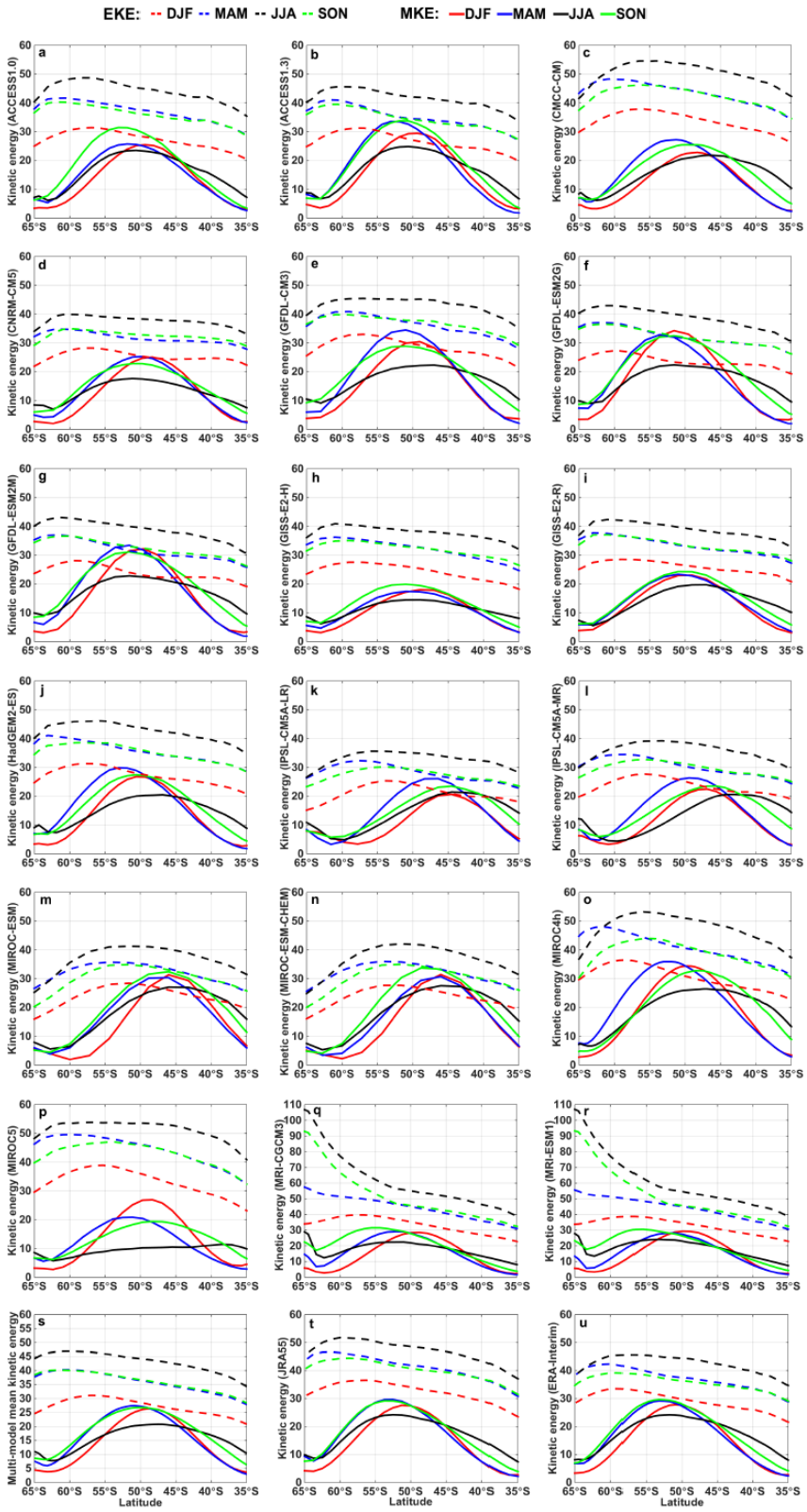

815

816 FIG. 6. The 1979-2005 seasonal-mean and zonal-mean mean kinetic energy (solid; $m^2 s^{-2}$)
817 and eddy kinetic energy (dashed; $m^2 s^{-2}$) from (a)-(r) the eighteen CMIP5 models, (s) their
818 multi-model mean, (t) JRA-55 and (u) ERA-Interim.

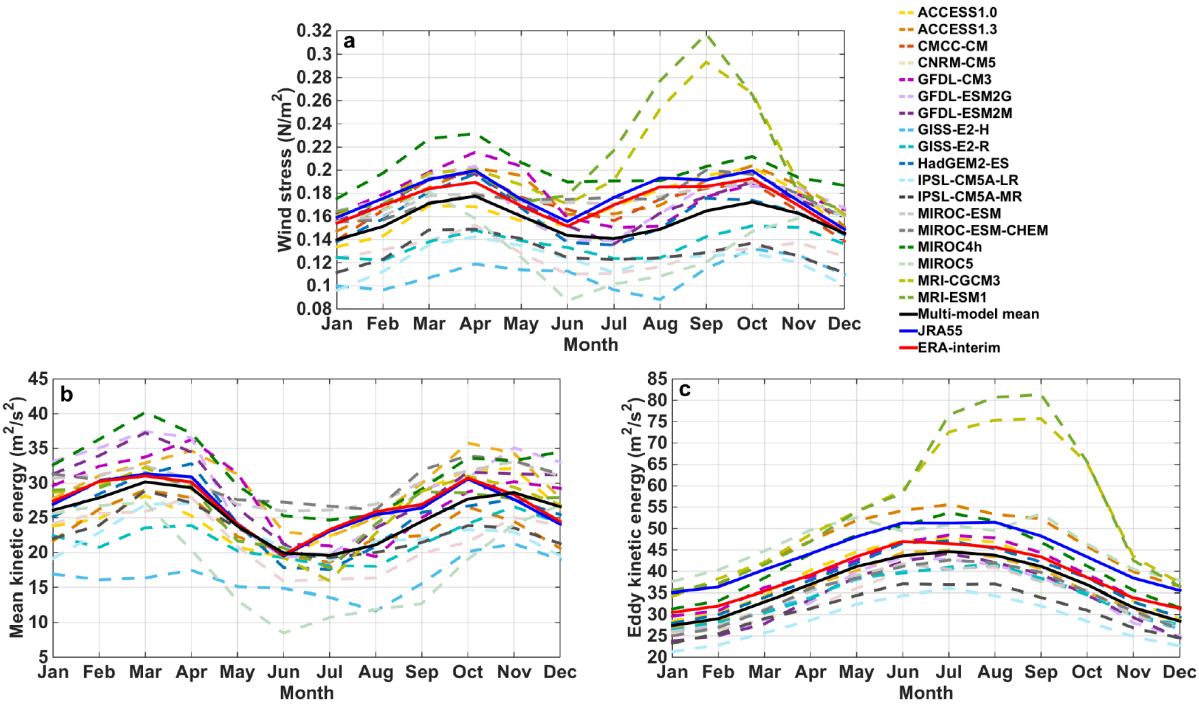

819

820 FIG. 7. Seasonal variability of (a) the peak values of 1979-2005 monthly-mean and zonal-
821 mean zonal wind stress $\tau_{>6hr}$ (N m^{-2}), (b) mean kinetic energy (m^2 s^{-2}) and (c) eddy kinetic
822 energy (m^2 s^{-2}) over the SO (35^o-65^{o}S) from the eighteen CMIP5 models (dashed), their
823 multi-model mean (solid black), JRA-55 (solid blue) and ERA-Interim (solid red).

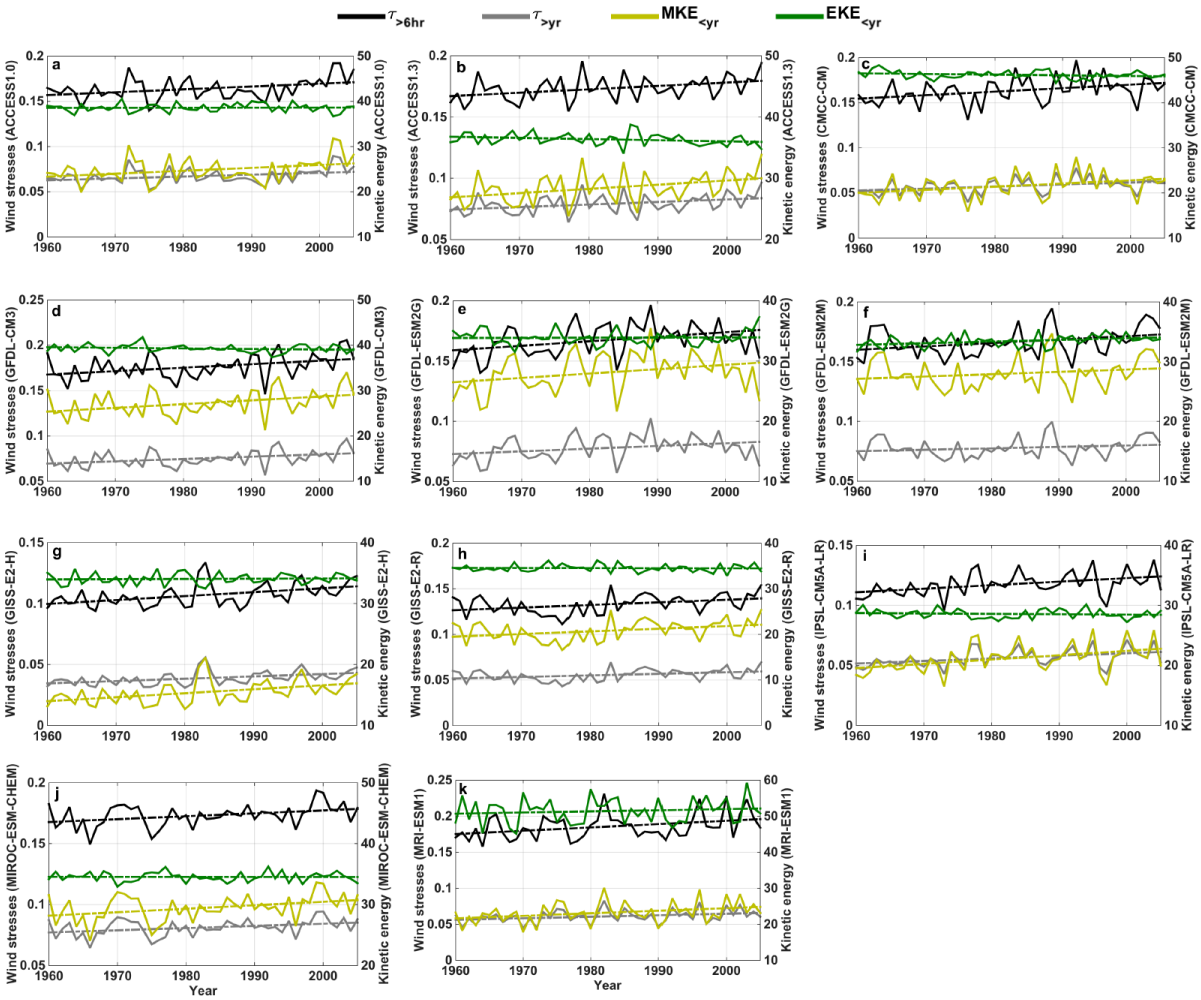

FIG. 8. Peak annual-mean and zonal-mean SO wind stresses $\tau_{>6hr}$ (black), $\tau_{>yr}$ (grey, N m^{-2}) and kinetic energy $MKE_{<yr}$ (yellow-green), $EKE_{<yr}$ (green, m^2 s^{-2}) at the position of peak annual-mean and zonal-mean $\tau_{>6hr}$ from 1960 to 2005 in the eleven CMIP5 models. The dash-dotted lines represent corresponding trends. Trends of $\tau_{>6hr}$ are significant in all eleven models, trends of $\tau_{>yr}$ and $MKE_{<yr}$ are significant in all eleven models except for GFDL-ESM2M, and the trend of $EKE_{<yr}$ is only significant in GFDL-ESM2M (see Table 3).